University of Kent

# Kent Academic Repository

**Zambetti, Noemi A, Ping, Zhen, Chen, Si, Kenswil, Keane J G, Mylona, Maria A, Sanders, Mathijs A, Hoogenboezem, Remco M, Bindels, Eric M J, Adisty, Maria N, Van Strien, Paulina M H and others (2016) *Mesenchymal Inflammation Drives Genotoxic Stress in Hematopoietic Stem Cells and Predicts Disease Evolution in Human Pre-leukemia*. Cell stem cell, 19 (5). pp. 613-627. ISSN 1875-9777.**

## Downloaded from

https://kar.kent.ac.uk/115042/ The University of Kent's Academic Repository KAR

## The version of record is available from

## This document version

Author's Accepted Manuscript

## DOI for this version

## Licence for this version

CC BY-ND (Attribution-NoDerivatives)

## Additional information

## Versions of research works

### Versions of Record

If this version is the version of record, it is the same as the published version available on the publisher's web site. Cite as the published version.

### Author Accepted Manuscripts

If this document is identified as the Author Accepted Manuscript it is the version after peer review but before type setting, copy editing or publisher branding. Cite as Surname, Initial. (Year) 'Title of article'. To be published in ***Title of Journal*** , Volume and issue numbers [peer-reviewed accepted version]. Available at: DOI or URL (Accessed: date).

## Enquiries

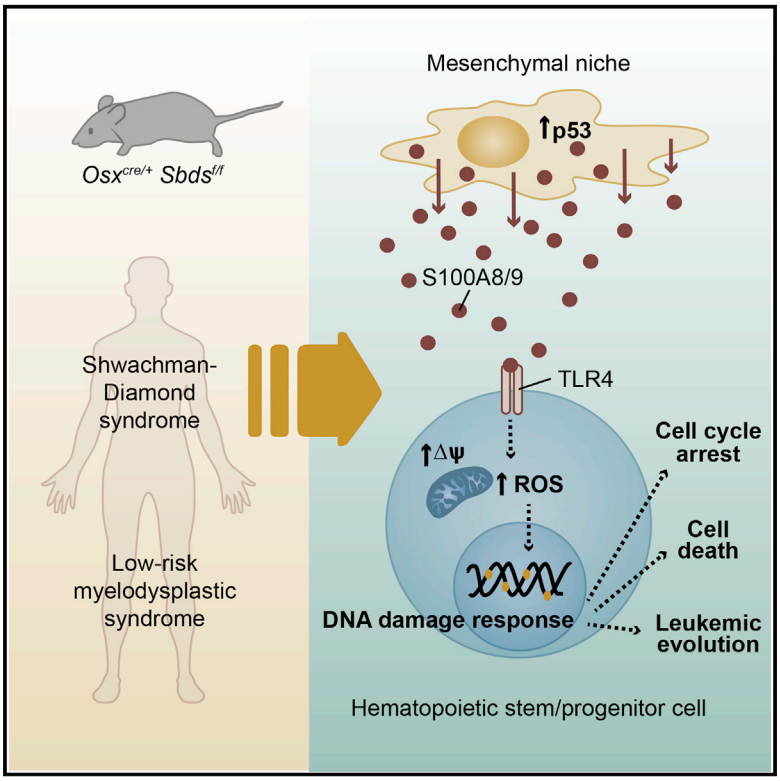
If you have questions about this document contact ResearchSupport@kent.ac.uk. Please include the URL of the record in KAR. If you believe that your, or a third party's rights have been compromised through this document please see our Take Down policy (available from https://www.kent.ac.uk/guides/kar-the-kent-academic-repository#policies).

Article

Cell Stem Cell

# Mesenchymal Inflammation Drives Genotoxic Stress in Hematopoietic Stem Cells and Predicts Disease Evolution in Human Pre-leukemia

## Graphical Abstract




## Authors

Noemi A. Zambetti, Zhen Ping, Si Chen, ..., Arjan A. van de Loosdrecht, Thomas Vogl, Marc H.G.P. Raaijmakers

## Correspondence

m.h.g.raaijmakers@erasmusmc.nl

## In Brief

Cell-extrinsic factors driving malignant transformation remain understudied. In a mouse model of pre-leukemia, Zambetti and colleagues establish a concept of mesenchymal niche-induced genotoxic stress in hematopoietic stem cells through p53-S100A8/9-TLR4 signaling, with relevance to human leukemia. The findings provide conceptual and mechanistic insights into the link between inflammation and cancer.

## Highlights

- Mesenchymal deletion of *Sbds* in mice recapitulates bone defects in SDS
- Mesenchymal niche cells induce genotoxic stress in HSPCs in this model
- p53-S100A8/9-TLR4 signaling, activated in SDS and MDS, drives these phenotypes
- Mesenchymal S100A8/9 predicts leukemic evolution and disease outcome in human MDS

## Accession Numbers

E-MTAB-5023
PRJEB15060
EGAS00001001926

Zambetti et al., 2016, Cell Stem Cell *19*, 613–627
November 3, 2016 © 2016 Elsevier Inc.
http://dx.doi.org/10.1016/j.stem.2016.08.021

Cell Stem Cell
Article

# Mesenchymal Inflammation Drives Genotoxic Stress in Hematopoietic Stem Cells and Predicts Disease Evolution in Human Pre-leukemia

Noemi A. Zambetti,[1,8] Zhen Ping,[1,8] Si Chen,[1,8] Keane J.G. Kenswil,[1] Maria A. Mylona,[1] Mathijs A. Sanders,[1] Remco M. Hoogenboezem,[1] Eric M.J. Bindels,[1] Maria N. Adisty,[1] Paulina M.H. Van Strien,[1] Cindy S. van der Leije,[2] Theresia M. Westers,[3] Eline M.P. Cremers,[3] Chiara Milanese,[4] Pier G. Mastroberardino,[4] Johannes P.T.M. van Leeuwen,[2] Bram C.J. van der Eerden,[2] Ivo P. Touw,[1] Taco W. Kuijpers,[5] Roland Kanaar,[6] Arjan A. van de Loosdrecht,[3] Thomas Vogl,[7] and Marc H.G.P. Raaijmakers[1,9,*]

[1]Department of Hematology, Erasmus MC Cancer Institute, Rotterdam 3015CN, the Netherlands
[2]Department of Internal Medicine, Erasmus MC Cancer Institute, Rotterdam 3015CN, the Netherlands
[3]Department of Hematology, VU University Medical Center, Cancer Center Amsterdam, Amsterdam 1081HV, the Netherlands
[4]Department of Molecular Genetics, Erasmus MC Cancer Institute, Rotterdam 3015CN, the Netherlands
[5]Department of Pediatric Hematology, Immunology and Infectious Diseases, Emma Children's Hospital, Academic Medical Centre (AMC), University of Amsterdam (UvA), Amsterdam 1105AZ, the Netherlands
[6]Departments of Genetics and Radiation Oncology, Cancer Genomics Center, Erasmus MC Cancer Institute, Rotterdam 3015CN, the Netherlands
[7]Institute of Immunology, University of Münster, Münster 48149, Germany
[8]Co-first author
[9]Lead Contact
*Correspondence: m.h.g.raaijmakers@erasmusmc.nl
http://dx.doi.org/10.1016/j.stem.2016.08.021

## SUMMARY

**Mesenchymal niche cells may drive tissue failure and malignant transformation in the hematopoietic system, but the underlying molecular mechanisms and relevance to human disease remain poorly defined. Here, we show that perturbation of mesenchymal cells in a mouse model of the pre-leukemic disorder Shwachman-Diamond syndrome (SDS) induces mitochondrial dysfunction, oxidative stress, and activation of DNA damage responses in hematopoietic stem and progenitor cells. Massive parallel RNA sequencing of highly purified mesenchymal cells in the SDS mouse model and a range of human pre-leukemic syndromes identified p53-S100A8/9-TLR inflammatory signaling as a common driving mechanism of genotoxic stress. Transcriptional activation of this signaling axis in the mesenchymal niche predicted leukemic evolution and progression-free survival in myelodysplastic syndrome (MDS), the principal leukemia predisposition syndrome. Collectively, our findings identify mesenchymal niche-induced genotoxic stress in heterotypic stem and progenitor cells through inflammatory signaling as a targetable determinant of disease outcome in human pre-leukemia.**

## INTRODUCTION

Genotoxic stress results in the accumulation of DNA lesions in hematopoietic stem and progenitor cells (HSPCs) over the lifespan of an organism, contributing to tissue failure and malignant transformation (Jaiswal et al., 2014; Rossi et al., 2007). The pathophysiological insults underlying genomic stress in HSPCs, however, remain incompletely understood. Perturbed signaling from their surrounding microenvironment may be implicated, but this has not been experimentally defined.

Components of the bone marrow microenvironment have emerged as key regulators of normal and malignant hematopoiesis (Arranz et al., 2014; Hanoun et al., 2014; Medyouf et al., 2014; Schepers et al., 2015; Walkley et al., 2007). We, and others, have shown that primary alterations of the mesenchymal niche can induce myelodysplasia and promote the emergence of acute myeloid leukemia (AML) with cytogenetic abnormalities in HSPCs (Kode et al., 2014; Raaijmakers et al., 2010), thus introducing a concept of niche-driven oncogenesis in the hematopoietic system.

To provide insights into the mechanisms that underlie this concept, as well as their relevance for human disease, we modeled the human leukemia predisposition disorder Shwachman-Diamond syndrome (SDS), caused by constitutive homozygous or compound heterozygous loss-of-function mutations in the *SBDS* gene, required for ribosome biogenesis (Boocock et al., 2003; Finch et al., 2011). SDS is characterized by skeletal defects in conjunction with a striking propensity to develop myelodysplastic syndrome (MDS) and AML at a young age, with a cumulative probability of >30% at the age of 30 years and a median onset at 18 years (Alter, 2007; Donadieu et al., 2012). Hematopoietic cell intrinsic loss of *Sbds* does not result in MDS or leukemia (Rawls et al., 2007; Zambetti et al., 2015), supporting the notion that cell-extrinsic factors contribute to malignant transformation. Deletion of *Sbds* from mesenchymal cells expressing the mesenchymal progenitor marker osterix (*Sp7*) in the bone marrow induced apoptosis in HSPCs and myelodysplasia, but the molecular mechanisms driving these observations

and their relevance for human disease remained to be defined (Raaijmakers et al., 2010).

Here, we identify the endogenous damage-associated molecular pattern (DAMP) molecules S100A8 and S100A9, secreted from mesenchymal niche cells, as drivers of mitochondrial dysfunction, oxidative stress, and DNA damage response (DDR) activation in HSPCs, with clinical relevance to the pathogenesis and prognosis of human bone marrow failure and leukemia predisposition syndromes.

## RESULTS

### Deletion of *Sbds* from Mesenchymal Progentitor Cells Recapitulates Skeletal Abnormalities of Human SDS

SDS is characterized by bone abnormalities including low-turnover osteoporosis with reduced trabecular bone volume, low numbers of osteoblasts, and reduced amount of osteoid, leading to increased risk of fractures (Toiviainen-Salo et al., 2007). The cellular subsets driving these abnormalities and the underlying molecular mechanisms have remained largely undefined. We have previously shown that Cre-mediated deletion of *Sbds* from osterix$^{+}$ mesenchymal progenitor cells (MPCs) (*Sbds*$^{f/f}$ *Osx*$^{cre/+}$ mice, hereafter OCS$^{f/f}$ or mutants) disrupts the architecture of the marrow and cortical bone (Raaijmakers et al., 2010). Here, we first sought to better define the skeletal defects in these mice and their relevance to human disease.

OCS$^{f/f}$ mice presented growth retardation and reduced femur length compared to control *Sbds*$^{f/+}$ *Osx*$^{cre/+}$ (OCS$^{f/+}$) mice (Figures 1A and 1B) as observed in human patients (Aggett et al., 1980; Ginzberg et al., 1999). The runted phenotype was associated with a significantly limited lifespan, with lethality observed after the age of 4 weeks. Analyses were therefore performed in 3-week-old mice. The femur trabecular area was profoundly reduced in OCS$^{f/f}$ mice, with decreased bone volume, low number of trabeculae, increased trabecular spacing, and reduced numbers of osteoblasts compared to controls (Figures 1C–1G and 1I). The cortical bone of OCS mutants was also affected, as indicated by low bone mineral density values (Figures 1C, 1D, and 1H), attenuating the mechanical properties of the bone, which was found less resistant to fracture in three-point bending test (Figure 1J). A tendency for reduced stiffness in the long bones was also observed (Figure 1K). Taken together, the structural and mechanical defects indicate that *Sbds* deficiency in MPCs causes osteoporosis with a propensity for fracturing, in line with observations in SDS patients (Ginzberg et al., 1999; Mäkitie et al., 2004; Toiviainen-Salo et al., 2007). Impaired osteogenesis did not reflect a contraction of the bone MPC pool as shown by frequency of CFU-F and Osx::GFP$^{+}$ cells (Figures S1A and S1B), but rather impairment of terminal osteogenic differentiation as suggested by transcriptional profiling of prospectively isolated osterix-expressing (GFP$^{+}$) cells (Figure S1C). Transcriptional data confirmed deregulated expression of genes related to ribosomal biogenesis and translation (Figures S1D and S1E), in line with the established role of *Sbds* in ribosome biogenesis. Collectively, these data support a view in which bone abnormalities in SDS are caused by deficiency of *Sbds* in MPCs, which attenuates terminal differentiation toward matrix-depositing osteoblastic cells with a compensatory increase in the most primitive mesenchymal compartment.

### *Sbds* Deficiency in the Hematopoietic Niche Induces Mitochondrial Dysfunction, Oxidative Stress, and Activation of the DDR in HSPCs

Having established that the OCS mice represent a bona fide model for bone abnormalities in human disease, we next investigated the hematopoietic consequences of these environmental alterations. HSPC number was unaltered in OCS mice (Figures S2A–S2C), and HSPCs displayed global preservation of their transcriptional landscape after exposure to the *Sbds*-deficient environment (Figures S2D–S2F). Transcriptional network analysis, however, revealed significant overlap with signatures previously defined as predicting leukemic evolution of human CD34$^{+}$ cells (Li et al., 2011), including pathways signaling mitochondrial abnormalities (Figure 2A; Table S1). Mitochondrial dysfunction was confirmed by measuring the mitochondrial membrane potential ($\Delta\psi$), indicating hyperpolarization of the mitochondria (Figures 2B and 2C). Mitochondrial hyperpolarization can result in reverse electron transfer, leading to the production of superoxide radicals, which can be further converted into other reactive oxygen species (ROS) (Murphy, 2009). In line with this, a marked increase in intracellular ROS levels was found in OCS mutant HSPCs (Figure 2D), more specifically superoxide radicals derived from mitochondria as shown by dihydroethidium (DHE) staining (Figure S2G) (Owusu-Ansah et al., 2008; Stowe and Camara, 2009). ROS can undermine the genomic integrity of HSPCs by inducing DNA damage (Ito et al., 2006; Walter et al., 2015; Yahata et al., 2011), to which normal HSPCs react by activating the DDR and DNA repair pathways (Rossi et al., 2007). Indeed, HSPCs (LKS-SLAM) from OCS$^{f/f}$ mice displayed accumulation of Ser139-phosphorylated H2AX histone ($\gamma$H2AX), which forms at the sites of DNA damage (Figures 2E and S2H). Treatment of OCS mutant animals with the ROS scavenger N-acetylcysteine (NAC) resulted in partial reduction in the accumulation of $\gamma$H2AX (Figures S2I and S2J). Congruent with genotoxic effects of the mutant microenvironment, HSPCs displayed transcriptional modulation of DDR and DNA repair pathways (Table S2), including nucleotide excision repair programs, associated with ROS-induced lesions (Curtin, 2012) and signatures related to the master regulator of DDR and cell-cycle checkpoint activation ataxia telangiectasia and Rad3-related (ATR). Activation of the G1-S cell-cycle checkpoint, resulting in cell-cycle arrest, was suggested by depletion of S-phase transcriptional signatures (Figure 2F; Table S1), in vivo BrdU/Ki67 labeling (Figures 2G, 2H, and S2K), and downregulation of the Myc pathway, a critical regulator for this restriction point and the coordination of S-G2-M progression (Figure 2I; Table S3). Apoptosis of mutant HSPCs, as an alternative outcome of checkpoint activation, was earlier demonstrated (Raaijmakers et al., 2010). Together, the data indicate that the *Sbds*-deficient environment induces mitochondrial dysfunction, oxidative stress, DNA damage, and genotoxic stress in HSPCs leading to activation of DDR pathways and G1-S checkpoint activation, reminiscent of a model in which mitochondrial dysfunction underlies an escalating cycle of increased ROS and genotoxic damage (Sahin and Depinho, 2010).

Short term exposure to the genotoxic environment did not attenuate HSPC function in DNA repair proficient cells, as demonstrated by competitive transplantation experiments

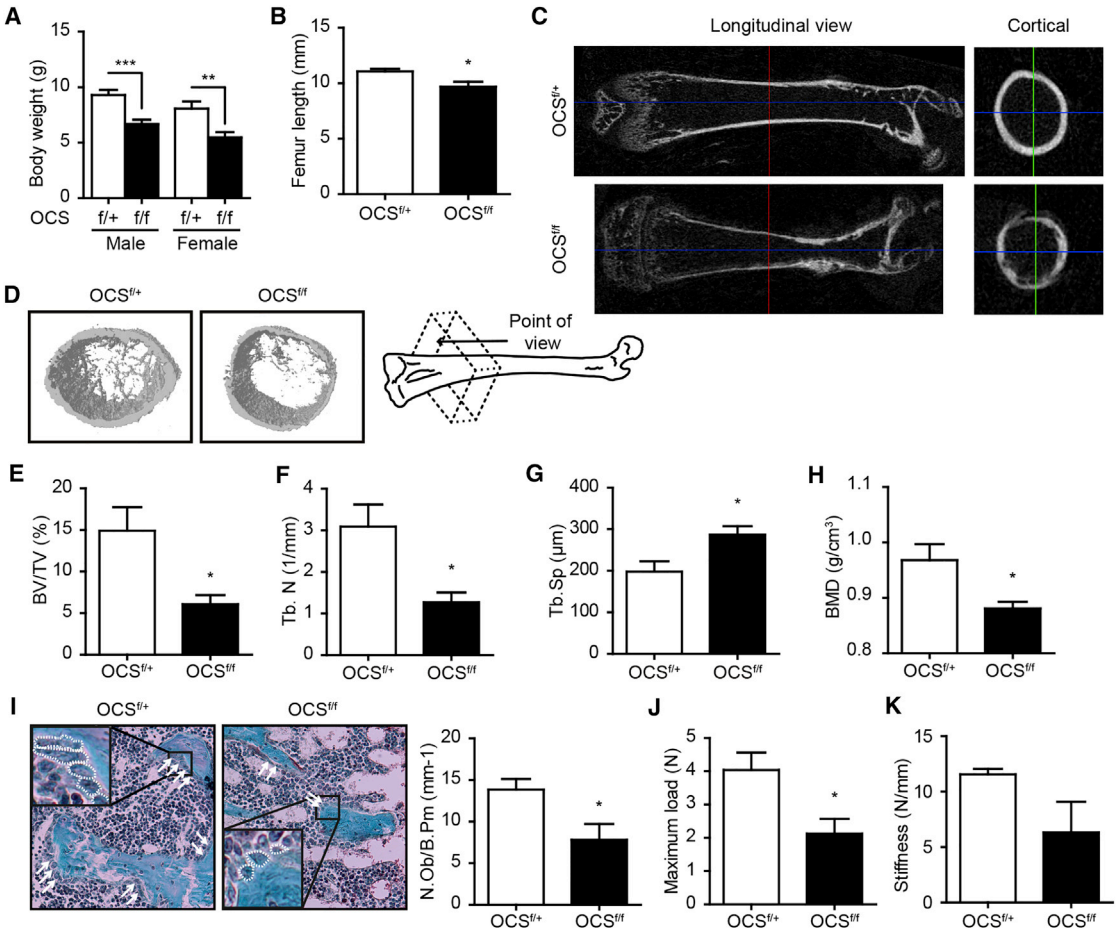



**Figure 1. Deletion of *Sbds* in MPCs Recapitulates Skeletal Defects in Human SDS**

(A and B) Impaired growth in $OCS^{f/f}$ mice: body weight (n = 9) (A) and femur length (n = 5) (B).

(C–H) Femur μCT analysis of $OCS^{f/+}$ (n = 5) and $OCS^{f/f}$ (n = 4) mice.

(C) Representative 2D images, left: longitudinal view and right: cortical bone.

(D) 3D image.

(E) Bone volume per tissue volume (BV/TV).

(F) Trabecular number (Tb. N).

(G) Trabecular spacing (Tb. Sp).

(H) Cortical bone mineral density (BMD).

(I) Goldner osteoblast staining ($OCS^{f/+}$, n = 6 and $OCS^{f/f}$, n = 8). The representative images (arrows: osteoblasts; with white dashed line in the magnified region) are shown (left). The number of osteoblasts per bone perimeter (N.Ob/B.Pm) is shown (right).

(J and K) 3-point bending test indicating reduced resistance to fracture (J) and decreased stiffness of $OCS^{f/f}$ bone (K) ($OCS^{f/+}$, n = 5 and $OCS^{f/f}$, n = 4) (*$p < 0.05$, **$p < 0.01$, and ***$p < 0.001$). The data are mean ± SEM.

See also Figure S1.

(Figures S3A–S3C), suggesting efficient DNA-repair or elimination of functionally impaired HSPCs by the DDR-driven apoptosis and cell-cycle arrest. Congruent with this notion, alkaline comet assays on sorted HSPCs failed to demonstrate structural DNA damage (Figures S3D and S3E).

## Activation of the p53 Pathway Drives Bone Abnormalities and Genotoxic Stress in OCS Mice

Next, we sought to define the molecular programs underlying the bone and hematopoietic alterations in OCS mice. A proposed common molecular mechanism for the pathogenesis of ribosomopathies involves activation of the p53 tumor suppressor pathway (Raiser et al., 2014). The p53 protein was overexpressed in $GFP^+$ MPCs in OCS mutants, with activation of downstream transcriptional pathways and upregulation of canonical targets (Figures 3A–3C). To assess the pathophysiological role of p53 activation in MPCs, we intercrossed OCS with *Trp53*-floxed mice (Marino et al., 2000), generating a double conditional knockout model where the deletion of p53 is localized in the *Sbds*-deleted stromal compartment ($Sbds^{f/f}$ $Trp53^{f/f}$ $Osx^{cre/+}$ mice; hence $OCS^{f/f}$ $p53^{\Delta}$) (Figure 3D). Genetic recombination of the *Trp53* locus was detected only in bone cells-containing samples, demonstrating the tissue specificity of p53 deletion in this model (Figure 3E). Genetic deletion of p53 from *Sbds*-deficient

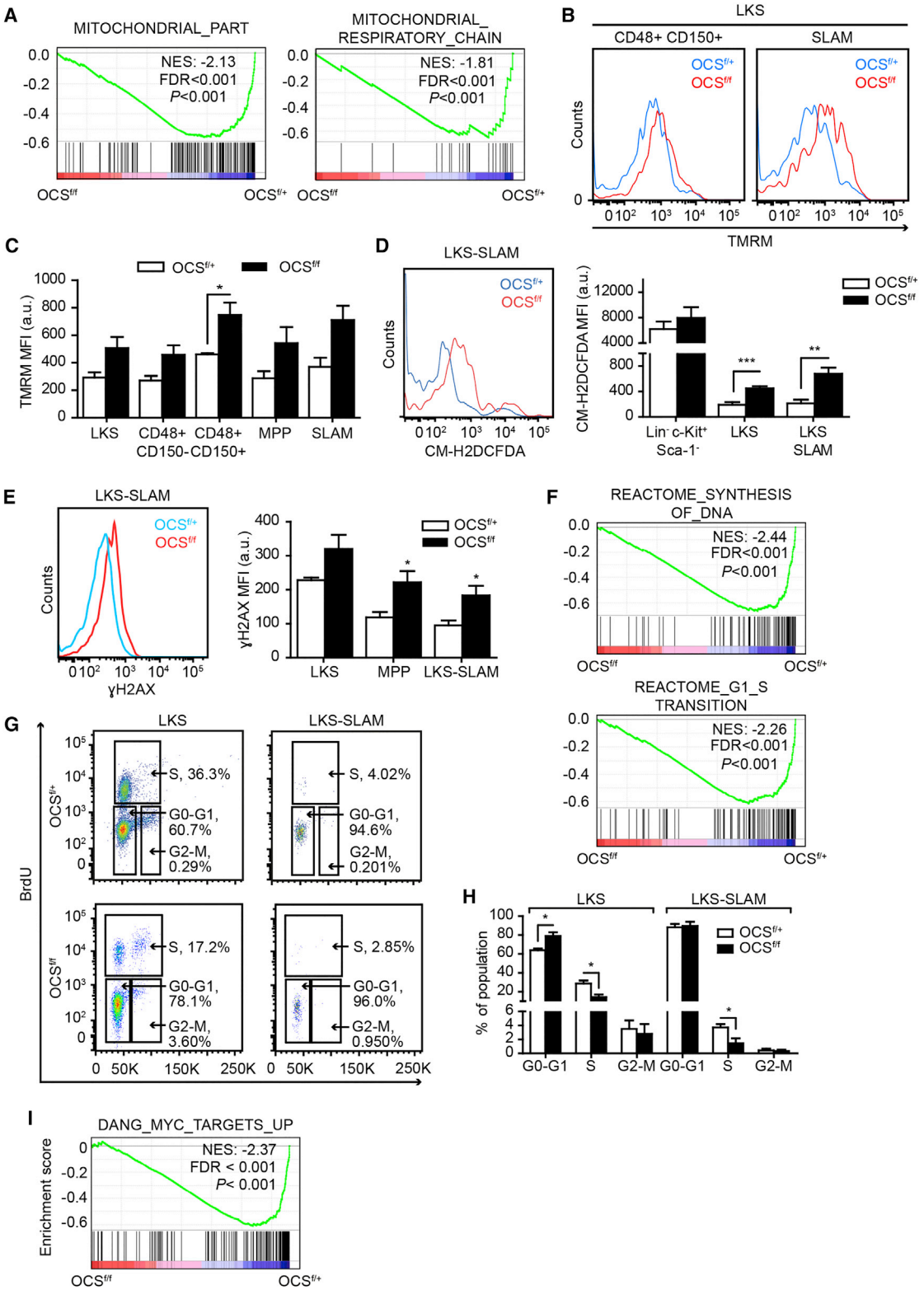



**Figure 2. *Sbds*-Deficient Mesenchymal Cells Induce Genotoxic Stress in HSPCs**

(A) Transcriptional network analysis indicating mitochondrial dysregulation in mutant HSPCs. normalized enrichment score: NES.

(B and C) Increased mitochondrial potential (TMRM) in HSPCs: representative plots (B); mean fluorescence intensity (MFI) (C) (n = 3).

(D) ROS quantification by CM-H2DCFDA ($OCS^{f/+}$, n = 6 and $OCS^{f/f}$, n = 7).

*(legend continued on next page)*

MPCs rescued the osteoporotic phenotype (Figures 3F–3J), but not cortical bone mineralization (Figure 3K), while it had only modest effects on bone mass in OCS control mice (Figure S4), in line with earlier observations (Wang et al., 2006). Rescue of the skeletal phenotype was linked to amelioration of genotoxic stress in HSPCs, as demonstrated by a reduction of superoxide radicals derived from mitochondria and DNA damage (Figures 3L and 3M).

## Identification of the DAMP Genes *S100A8* and *S100A9* as Candidate Niche Factors Driving Genotoxic Stress in Human Leukemia Predisposition Syndromes

To identify human disease-relevant niche factors, downstream of p53 activation, driving genomic stress in HSPCs, we compared the transcriptomes of GFP$^+$ MPCs from OCS mice to those from prospectively fluorescence-activated cell sorting (FACS)-isolated mesenchymal CD271$^+$ niche cells (Tormin et al., 2011) from human SDS patients (Figure 4A; Table S4). The mesenchymal nature of CD271$^+$ cells was confirmed by CFU-F capacity and differential expression of mesenchymal, osteolineage, and HSPC-regulatory genes (Chen et al., 2016). RNA sequencing showed the presence of *SBDS* mutations (Figures 4B and S5; Table S4) associated with reduced *SBDS* expression (Figure 4C), confirming molecular aspects of SDS in previous studies (Finch et al., 2011; Woloszynek et al., 2004). Virtually identical transcriptional signatures of disrupted ribosome biogenesis and translation were found in human niche cells (Figure 4D) and in GFP$^+$ cells from OCS mice (Figure S1E), confirming faithful recapitulation of human molecular disease characteristics in the mouse model. There were 40 genes that were differentially expressed both in the mouse model and human SDS, 25 of which were overexpressed, with a remarkable abundance of genes encoding proteins implicated in inflammation and innate immunity (Figure 4E).

To further delineate candidate genes driving genomic stress and leukemic evolution from this gene set, we performed whole transcriptome sequencing of CD271$^+$ cells in two related human bone marrow failure and leukemia predisposition disorders: (1) low-risk MDS, the principal human pre-leukemic disorder in which cell-cycle exit (senescence), accumulation of ROS, DNA damage, and apoptosis have been described (Head et al., 2011; Peddie et al., 1997; Xiao et al., 2013), reminiscent of HSPC phenotypes in OCS mice and (2) DBA, like SDS, a ribosomopathy characterized by bone marrow failure, but with a much lower propensity to evolve into AML (<1% with longer latency than observed in SDS and MDS) (Vlachos et al., 2012) (Table S4). We reasoned that genes specifically overexpressed in mesenchymal niche cells from disorders with as strong propensity for leukemic evolution (SDS and MDS) might represent strong candidate drivers of genotoxic stress. We found 11 such genes (Figure 4F), among which were the DAMP genes *S100A8* and *S100A9*, which were significantly ($p < 0.05$) differentially expressed in GFP$^+$ cells from OCS mutant mice (Figures 4E–4G) and also represent a bona fide downstream transcriptional target of p53 (Li et al., 2009). Ex vivo small hairpin (sh)RNA experiments confirmed that upregulation of both p53 and S100A8/9 are direct, cell-intrinsic consequences of *Sbds* downregulation in mesenchymal precursor (OP9) cells (Figure S6A).

## Niche-Derived S100A8/9 Induces Genotoxic Stress in Murine and Human HSPCs

*S100A8* and *S100A9* belong to a subclass of proinflammatory molecules referred to as DAMP or alarmins. DAMPs are endogenous danger signals that are passively released or actively secreted in the microenvironment after cell death, damage, or stress and bind pattern recognition receptors (PRR) to regulate inflammation and tissue repair (Srikrishna and Freeze, 2009). S100A8 and S100A9 proteins were overexpressed in mouse *Sbds*-deficient MPCs (Figures 5A and 5B) and increased plasma concentration of S100A8/9 indicated secretion of the heterodimer (Figure 5C). Its canonical receptor TLR4 (Vogl et al., 2007) is expressed in murine HSPCs (Figure S6B), and the canonical downstream signaling NF-κB and MAPK pathways were activated in HSPCs from OCS$^{f/f}$ mice (Figure S6C).

Exposure of HSPCs (LKS) to recombinant murine S100A8/9 resulted in increased DNA damage (number of γH2AX and 53BP1 foci) (Figures 5D and S6D), which was replication independent (Figure 5E), and apoptosis (Figure 5F), associated with activation of TLR signaling (Figure 5G; Table S5), recapitulating the in vivo HSPC phenotype (Raaijmakers et al., 2010). In vivo, blockage of TLR4 by neutralizing antibodies resulted in a reduction of γH2AX foci in LKS cells from OCS$^{f/f}$ mice (Figure 5H).

To provide formal experimental support for the view that S100A8/9 production by ancillary cells in the bone marrow microenvironment is sufficient to drive genotoxic stress in HSPCs in a paracrine manner, we next transplanted CD45.1$^+$ wild-type hematopoietic cells into S100A9-GFP transgenic (S100A9Tg) mice, overexpressing both *S100A8* and *S100A9* under control of the MHC class I H2K promoter (Cheng et al., 2008) (Figure 6A). S100A8/9 (GFP) was expressed in a mesenchymal (CD45$^-$ CD31$^-$ Ter119$^-$ CD51$^+$ Sca1$^-$) niche population, previously shown to contain the Osterix-expressing cells (Schepers et al., 2013) (Figures 6B and 6C). The S100A8/9$^+$ microenvironment induced accumulation of superoxide radicals (DHE) and DNA-damage (γH2AX) in wild-type (CD45.1$^+$) HSPCs (Figures 6D–6F), in particular in immunophenotypic HSCs, indicating that secretion of S100A8/9 from ancillary cells in the microenvironment is indeed sufficient to induce genotoxic stress in HSCs in a paracrine manner.

(E) Increased γH2AX levels in mutant HSPCs. The representative FACS analysis is shown (left). The MFI values (n = 4) are shown (right).
(F–I) Activation of DDR in mutant HSPCs.
(F) Transcriptional repression of G1-S checkpoint progression.
(G and H) In vivo BrdU staining confirming impaired S-phase transition (n = 4).
(I) Downregulation of Myc signaling. GSEA data shown are from CD48$^-$ LKS cells. a.u., arbitrary units. ($^{\dagger\dagger\dagger}$FDR < 0.001, *p < 0.05, **p < 0.01, and ***p < 0.001). The data in bar graphs are mean ± SEM.
See also Figures S2, S3, and S6 and Tables S1, S2, and S3.

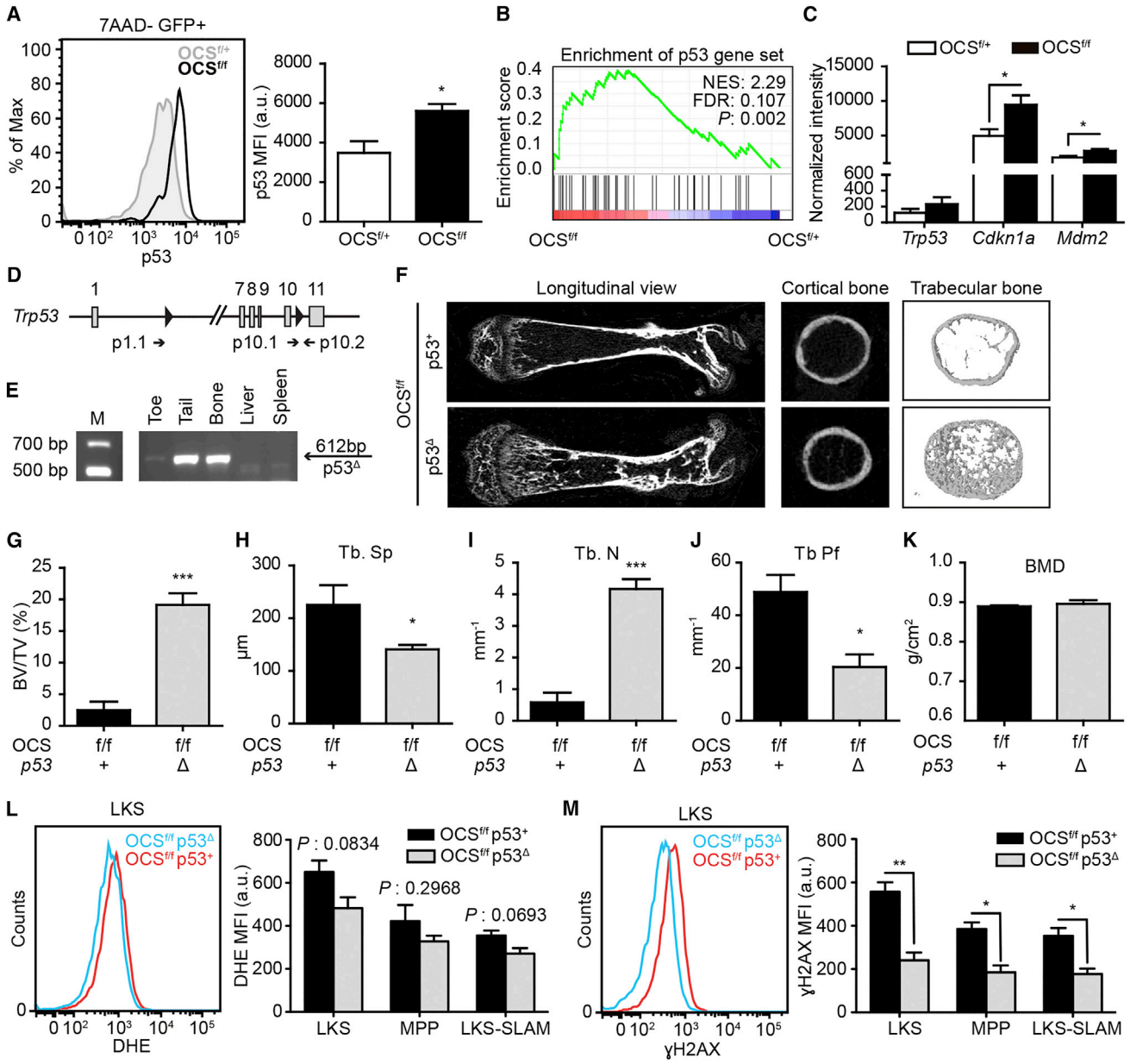



**Figure 3. Activation of p53 in MPCs Drives Skeletal and Hematopoietic Abnormalities in OCS Mutants**

(A) p53 protein (FACS) accumulates in GFP$^+$ cells from OCS$^{f/f}$ mice (n = 3).

(B and C) Activation of p53 in mutant GFP$^+$ cells as demonstrated by enrichment of a p53 GSEA signature (B) and overexpression of canonical p53 targets (n = 3) (C).

(D) Schematic representation of the p53 floxed allele with indication of primers used to assess genotypes (p10.1–p10.2) and genomic deletion (p1.1–p10.2).

(E) Specific deletion of p53 in bone-containing tissue in OCS$^{f/f}$ p53$^{\Delta}$ mice (genomic PCR).

(F–J) Non-compiled μCT images indicating normalization of bone mass in OCS$^{f/f}$ mice upon genetic deletion of p53 (p53$^+$, n = 3 and p53$^{\Delta}$, n = 5). trabecular bone pattern factor, Tb. Pf.

(K) Bone mineral density in OCS$^{f/f}$ mice is not rescued by p53 deletion.

(L and M) Effects of p53 deficiency on OCS HSPCs. The tendency for reduced oxidative stress as assessed by DHE analysis (L) and significant reduction of γH2AX levels (M) in HSPCs from OCS$^{f/f}$ p53$^{\Delta}$ mice (n = 3). Mean fluorescence intensity, MFI and a.u. (*p < 0.05, **p < 0.01, and ***p < 0.001). The data are mean ± SEM. See also Figure S4.

Translating these findings to human disease, exposure of human cord blood CD34$^+$ HSPCs to human recombinant S100A8/9 at clinically relevant concentrations (Chen et al., 2013 and Supplemental Information) resulted in DNA damage (increased γH2AX foci), apoptosis, and impaired HSPC function (CFU-C) (Figure S7).

## Activation of the p53-S100A8/9-TLR Axis in Mesenchymal Niche Cells Predicts Leukemic Evolution and Clinical Outcome in Human Low-Risk MDS

To further define the biologic and clinical significance of these findings, we performed transcriptome sequencing of CD271$^+$

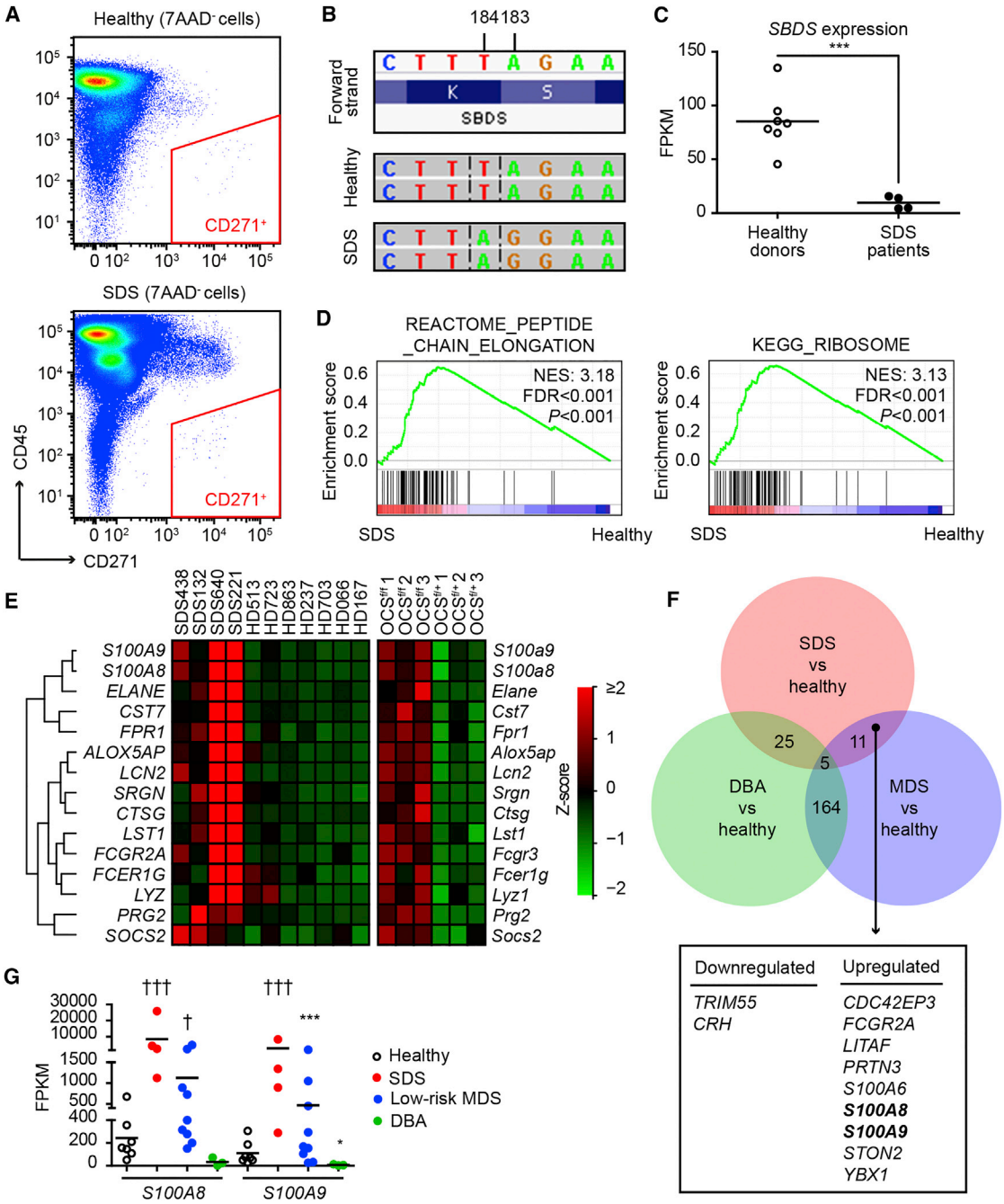



**Figure 4. Identification of *S100A8* and *S100A9* as Candidate Drivers of Genotoxic Stress in Leukemia Predisposition Syndromes**

(A) Representative mesenchymal CD271$^+$ FACS gating.

(B) Pathognomonic 183–184 TA > CT mutation in niche cells from a representative SDS patient (IGV plot).

(C) Reduced *SBDS* expression in SDS niche cells.

(D) Disruption of ribosome biogenesis and translation in SDS CD271$^+$ cells (GSEA).

(E) Inflammation-related transcripts are upregulated in niche cells from SDS patients and OCS$^{f/f}$ mice.

(F) Significantly differentially expressed genes in SDS (n = 4), MDS (n = 9), and DBA (n = 3) in comparison to normal CD271$^+$ cells.

(G) Expression of *S100A8* and *S100A9* in mesenchymal cells from SDS, low-risk MDS, and DBA patients (*p < 0.05, ***p < 0.001, and $^{\dagger\dagger\dagger}$FDR-adjusted p < 0.001). See also Figures S1 and S5 and Table S4.

niche cells in a prospective, homogeneously treated cohort of low-risk MDS patients (n = 45; Figure 7A; Table S6). Expression of *S100A8* and *S100A9* was strongly correlated (Figures 7B and 7C), with a subgroup of MDS patients (17/45; 38%) demonstrating significant overexpression of *S100A8* and *S100A9* (Modified Thompson Tau outlier test) (Figures 7B and 7D),

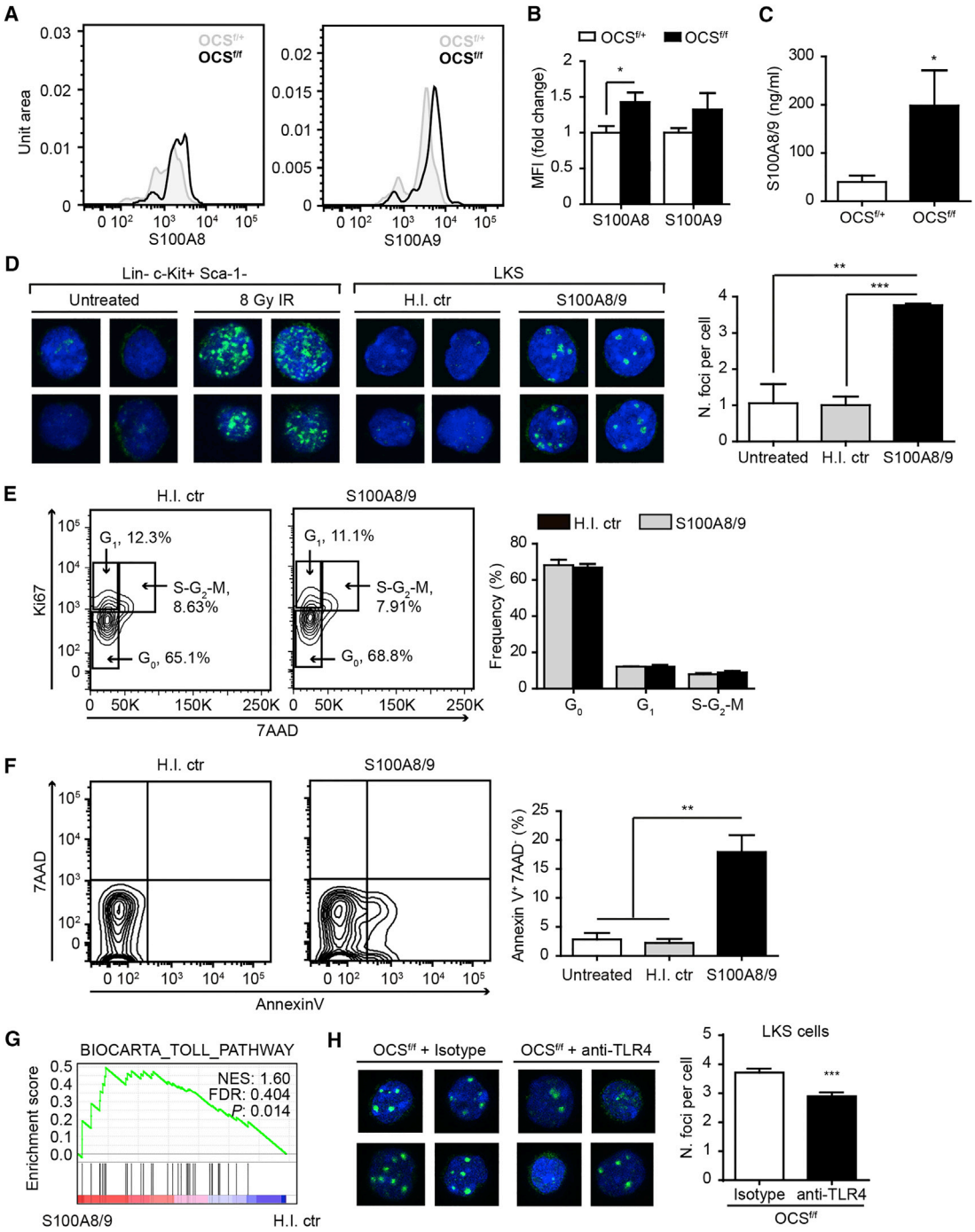



**Figure 5. S100A8/9 Induces Genotoxic Stress in Murine HSPCs through TLR4 Signaling**

(A and B) Increased S100A8 and S100A9 levels in $OCS^{f/f}$ $GFP^+$ cells.

(A) Representative plots.

(B) MFI values (n = 5).

(C) Increased plasma concentration of S100A8/9 by ELISA ($OCS^{f/+}$, n = 5 and $OCS^{f/f}$, n = 4).

(D) Left: representative γH2AX pictures after HSPCs in vitro exposure. Positive control: 8-Gy irradiated $Lin^-$ $c\text{-}Kit^+$ $Sca\text{-}1^-$ cells and negative control: heat-inactivated S100A8/9 (H.I. ctr). The number of γH2AX foci (n = 3) (right).

(E) S100A8/9 has no effect on cell cycle (n = 2).

(F) Increased apoptosis in S100A8/9-exposed LKS (n = 3).

(G) Activation of TLR signaling (GSEA).

(H) TLR4-blocking antibodies limit DNA damage in $OCS^{f/f}$ mice (n = 4) (*p < 0.05, *p < 0.01, and ***p < 0.001). The data are mean ± SEM.

See also Figures S6 and S7 and Table S5.

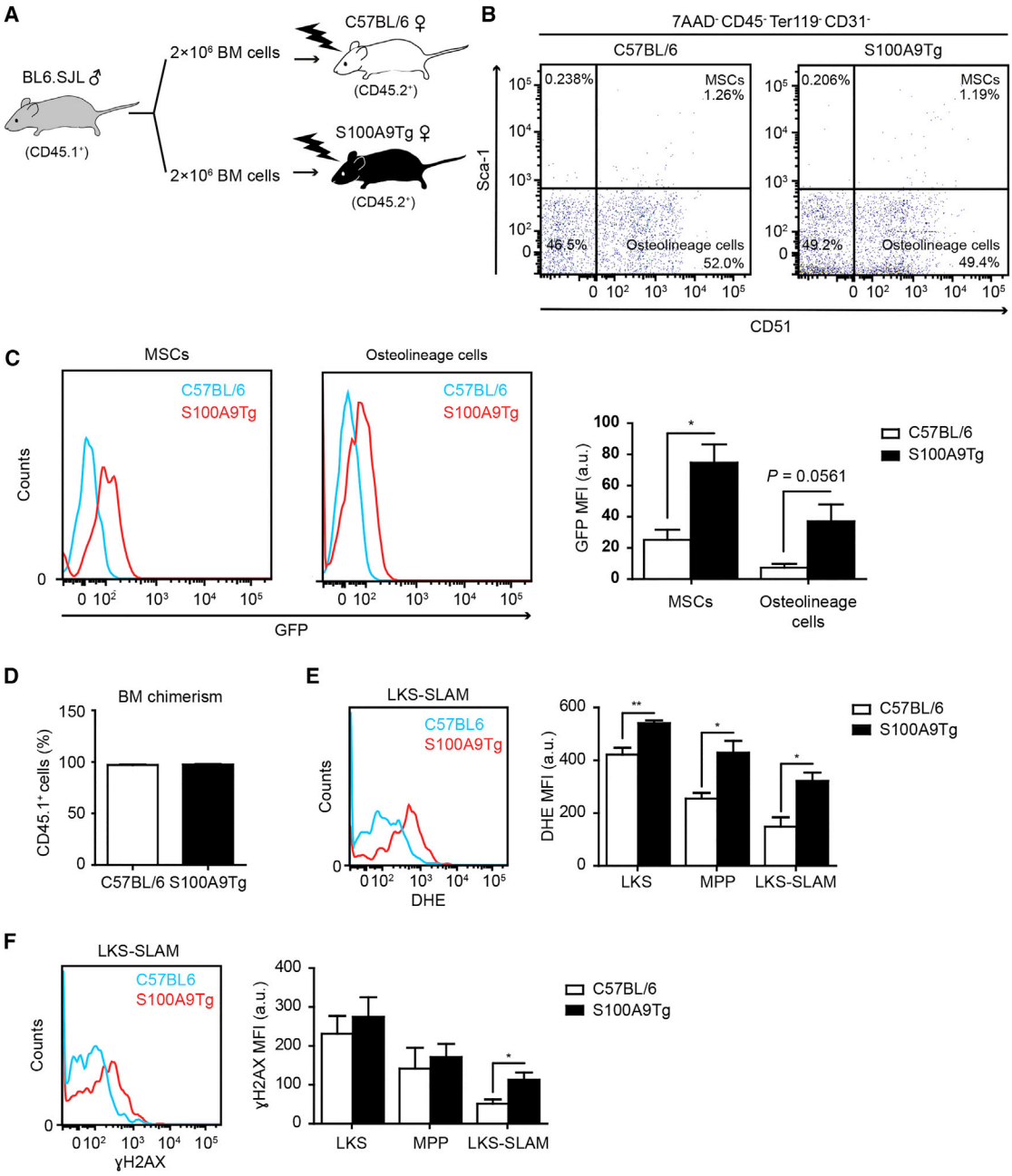



**Figure 6. Niche-Derived S100A8/9 Induces Oxidative and Genotoxic Stress in HSPCs**

(A) Schematic representation of wild-type HSPCs transplantation in S100A9Tg mice. Bone marrow, BM.

(B and C) Mesenchymal cells from S100A9Tg mice express the S100A9-IRES-GFP construct.

(B) Gating strategy defining CD51$^+$ Sca-1$^+$ mesenchymal "stem" cells (MSC) and CD51$^+$ Sca-1$^-$ osteolineage cells in the microenvironment.

(C) Expression of GFP in S100A9Tg-derived mesenchymal compartments (n = 3).

(D) Transplantation efficiency as assessed by CD45.1$^+$ cell chimerism in the bone marrow (BM) of transplanted mice (n = 4).

(E) Accumulation of superoxide radicals in HSPCs exposed to S100A8/9-overexpressing microenvironment. The representative plot is shown (left). DHE MFI values are shown (n = 4) (right).

(F) Increased levels of γH2AX in immunophenotypically defined HSCs. The representative plot is shown (left). The γH2AX MFI values are shown (n = 4) (right) (*p < 0.05 and **p < 0.01). The data are mean ± SEM.

independent of established prognostic factors as defined by the revised International Prognostic Scoring System (IPSS) and the MD Anderson risk score (LR-PSS) (Table S6). Transcriptional pathway analysis (GSEA) comparing mesenchymal cells overexpressing S100A8/9 (n = 17) to those of niche S100A8/9$^-$ patients (n = 28) revealed activation of p53 and TLR programs in S100A8/9$^+$ mesenchymal cells (Figure 7E), in line with experimental data from the mouse model pointing at the existence of a

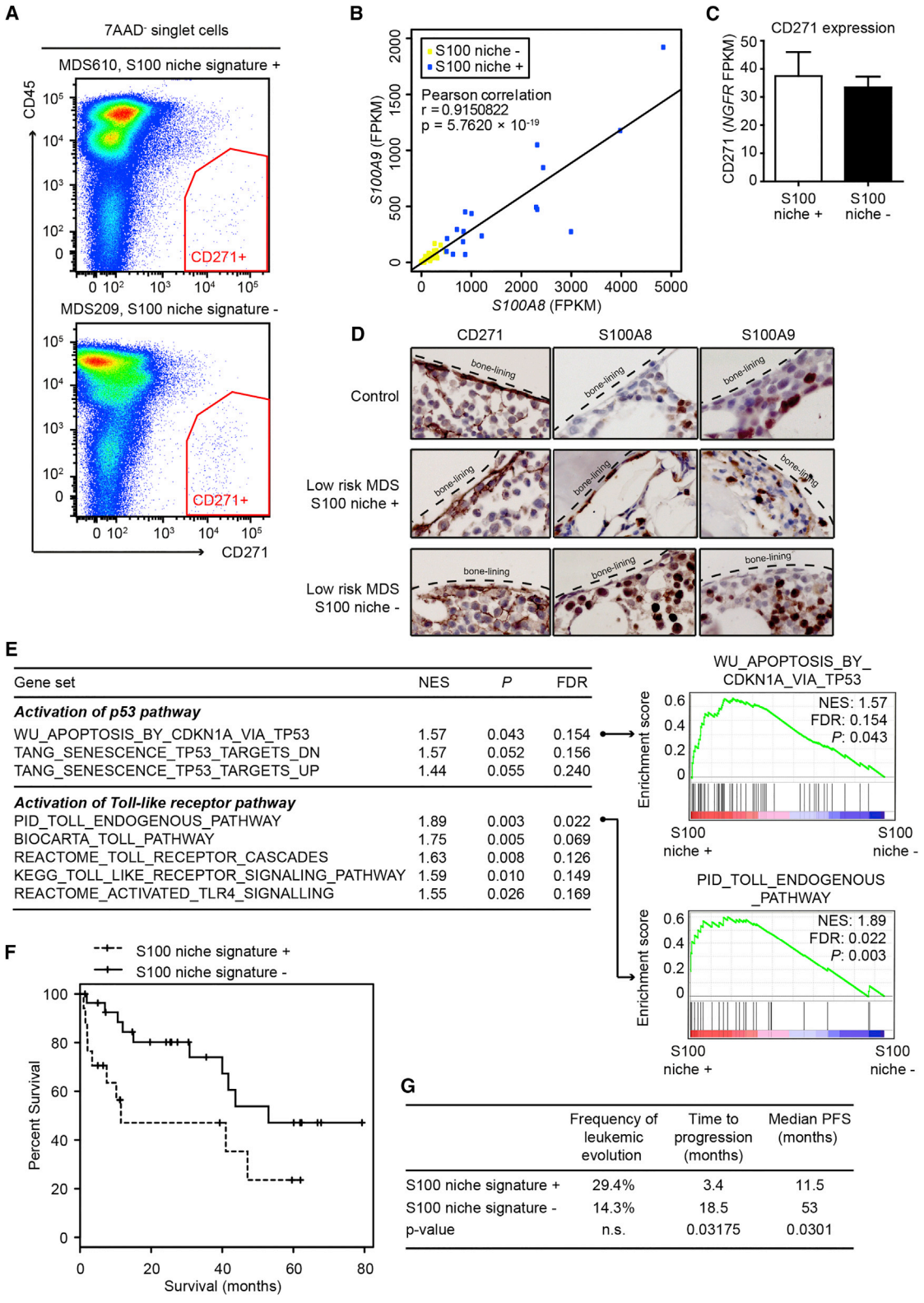



**Figure 7. Activation of the p53-S100A8/9-TLR Axis in Mesenchymal Niche Cells Predicts Leukemic Evolution and Clinical Outcome in Human Low-Risk MDS**

(A) Representative examples of FACS-isolated CD271$^+$ niche cells in human low-risk MDS.

(B) Correlation plot of *S100A8* and *S100A9* expression levels in human low-risk MDS (n = 45).

*(legend continued on next page)*

p53-S100A8/9-TLR axis. Leukemic evolution, defined as the development of frank AML or excess of blasts to World Health Organization (WHO) refractory anemia with excess of blasts (RAEB)1/ RAEB2, occurred in 5/17 (29.4%) of niche S100A8/9$^+$ patients (three AML and two RAEB1/RAEB2) versus 4/28 (14.2%) in niche S100A8/9$^-$ patients (two AML and 2 RAEB1/ RAEB2). Time to leukemic evolution was significantly shorter in niche S100A8/9$^+$ patients (average 3.4 [1–7.5] versus 18.5 [7–40] months; p = 0.03 by Exact Wilcoxon rank-sum test), resulting in a significantly shorter progression-free survival of niche S100A8/9$^+$ patients (median 11.5 versus 53 months; p = 0.03) (Figures 7F and 7G). Collectively, the data establish activation of p53-S100A8/9 signaling in mesenchymal niche cells as an independent predictor of disease outcome in human MDS.

## DISCUSSION

Genomic stress and the ensuing DNA damage play a pivotal role in the attenuation of normal hematopoiesis in aging and disease. Mutations accumulate in HSPCs over the lifespan of an organism, but the (patho)physiological sources of genomic stress in HSPCs and their relationship with human bone marrow failure remain incompletely understood. Here, we show that specific inflammatory signals from the mesenchymal niche can induce genotoxic stress in heterotypic stem/progenitor cells and relate this concept to the pathogenesis of two human bone marrow failure and leukemia predisposition syndromes, SDS and MDS.

The data indicate that the mesenchymal niche may actively contribute to the formation of a "mutagenic" environment, adding to our understanding of how a premalignant environment facilitates cancer initiation and evolution. The data argue that this may not only occur through facilitated selection and expansion of genetic clones that stochastically emerge in a permissive environment, but that the mesenchymal niche may be an active participant in driving the genotoxic stress underlying tissue failure and malignant transformation of parenchymal cells.

Notably, leukemic transformation was not observed in mice with targeted deficiency of *Sbds* in mesenchymal cells. Earlier, in a related mouse model of targeted *Dicer1* deletion in MPCs, leukemic transformation was a rare event (Raaijmakers et al., 2010). In the light of our current findings, these observations are likely explained by several factors. First, prolonged exposure to a mutagenic niche, beyond the limited lifespan of OCS mice, may be necessary for the accumulation of genetic damage required for full transformation. Additionally, the data argue that DNA repair-proficient HSPCs are able to cope with the mutagenic stress induced by their environment through activation of the DDR (as shown by molecular activation of cell-cycle checkpoints and apoptosis), preventing the accumulation of stable genetic damage (as demonstrated by comet assays) and maintaining the functional integrity of HSPCs (as shown by repopulation assays).

We propose that in SDS (and possibly other congenital bone marrow failure syndromes), genetically aberrant hematopoietic and niche elements cooperate in driving bone marrow failure and leukemic evolution. Our mouse models of SDS support a view in which hematopoietic cell autonomous loss of function of *Sbds* drives neutropenia (Zambetti et al., 2015), while niche alterations in this disease drive myelodysplastic alteration and genotoxic stress. It is conceivable that loss-of-function mutations in *Sbds* in HSPCs further sensitize HSPCs to the genotoxic effects of the *Sbds*-deficient environment, perhaps through attenuation of DNA damage repair mechanisms. It will thus be of considerable interest to test the hypothesis that a mutagenic environment cooperates with aberrant HSPCs, compromised in their ability to cope with inflammatory genotoxic stress, in leukemia evolution. In this context, the propensity of *Sbds*-deficient cells to accumulate ROS (Ambekar et al., 2010), and their reduced ability to cope with various cellular stressors such as mitotic spindle destabilizing agents, ER stress activators, topoisomerase inhibitors, and UV irradiation (Austin et al., 2008; Ball et al., 2009), is noteworthy.

The current findings add to emerging insights into the role of innate immune TLR-signaling in the pathogenesis of human MDS. TLR4 and other TLRs are overexpressed in HSPCs from MDS patients (Maratheftis et al., 2007; Wei et al., 2013), and TLR4 expression was shown to correlate with apoptosis in CD34$^+$ hematopoietic cells. TLR signaling is constitutively activated in MDS mice with deletion of chromosome 5 (del5q) (Starczynowski et al., 2010), and multiple TLR downstream signaling pathways have been shown to be activated in MDS and related to loss of progenitor cell function (Gañán-Gómez et al., 2015).

Our findings implicate the DAMP S100A8/9 derived from the mesenchymal niche as a driver of TLR signaling in this disease. The unbiased identification of S100A8/9 seems to independently converge with an earlier report implicating S100A8/9 in the pathogenesis of MDS (Chen et al., 2013). In this study, it was shown that the plasma concentration of S100A9 was significantly increased in MDS patients (Chen et al., 2013), and S100A8/9 was shown to drive expansion and activation of myeloid-derived suppressor cells (MDSCs) that contributed to cytopenia and myelodysplasia in a murine model of S100A9 overexpression through secretion of suppressive cytokines. It is therefore an intriguing possibility that additional, indirect, biologic effects of S100A8/9 contribute to the hematopoietic phenotype of OCS mice. This may include engagement of other cognate receptors of the protein, including expansion of MDSCs through CD33 signaling (Chen et al., 2013).

In our study, S100A8/9 was aberrantly overexpressed in a rare population of mesenchymal niche cells, both in the mouse model

(C) Expression of the defining gene *NGFR* (CD271) in mesenchymal cells (S100 niche +, n = 17 and S100 niche −, n = 28).
(D) Representative staining of S100A8 and S100A9 in endosteal (CD271$^+$) stromal cells. The intramedullary staining reflects expression of S100A8/9 in myeloid cells.
(E) GSEA analysis indicating enrichment of p53 and TLR signatures in S100A8/9-overexpressing CD271$^+$ cells. Two representative GSEA plots are shown. Normalized enrichment score, NES.
(F) Kaplan-Meier survival curve showing progression-free survival.
(G) Statistical analysis indicating significantly reduced time to progression and progression-free survival (PFS). The data are mean ± SEM.
See also Table S6.

and human disease. Typically, expression of the protein is found in myeloid cells, raising the question why S100A8/9 production by (rare) niche cells is more relevant to the biology of HSPCs than secretion from myeloid/erythroid cells. While the answer to this question remains speculative in the absence of in vivo targeted overexpression studies, it is noteworthy that, in contrast to most cytokines, chemokines, and other proinflammatory molecules, the local accumulation of S100A8/9 in the environment is very high (up to 100 μg/mL and about 50- to 100-fold higher than systemic concentrations), likely caused by attachment to extracellular matrices such as proteoglycans (Vogl et al., 2014). This implicates that the exposure of HSPCs to S100A8/9 is projected to relate strongly to their anatomical proximity to a producing cell. $CD271^+$ mesenchymal cells are directly adjacent to $CD34^+$ HSPCs in human bone marrow (Flores-Figueroa et al., 2012). This notion of "spatial relevance" may also be congruent with recent observations that aberrant overexpression of S100A8/9 in hematopoietic (erythroid) cells within the erythroid island in a model of human $5q^-$ syndrome leads to a predominant erythroid, anemic, phenotype (Schneider et al., 2016).

The mechanisms of S100A8/9 induced DNA damage remain to be fully elucidated. Our experiments using NAC to reduce ROS burden suggest an incomplete association between oxidative stress and DNA damage, suggesting that S100A8/9 secretion may attenuate genomic integrity through additional mechanisms. Similarly, it is conceivable that other ligands secreted from mesenchymal cells contribute to the induction of DNA damage in HSPCs in the mouse model. We found a striking abundance of transcripts encoding other DAMPs and cytotoxic proteins in both the mouse model and mesenchymal elements isolated from SDS patients. Ongoing investigations will have to assess whether other selected ligands can evoke genomic stress in heterotypic HSPCs and in such a fashion contribute to the generation of a mutagenic environment in these disorders.

Finally, our findings establish molecular characteristics of the mesenchymal environment as an important determinant of disease outcome in humans. S100A8/9 expression, associated with activated p53 and TLR signaling, in mesenchymal cells predicted leukemic evolution and progression-free survival in a cohort of homogeneously treated low-risk MDS patients. This is of considerable clinical relevance because low-risk MDS is a heterogeneous disease-entity, with a subset of patients having a particular dismal prognosis not identified by current risk-stratification strategies (Bejar et al., 2012). Gene expression of S100A8/9 may identify a substantial subset of patients with a survival typically associated with "high-risk" patients and, if confirmed in larger independent cohorts, could guide therapeutic decision making in MDS. The data thus provide a strong rationale for niche-instructed therapeutic targeting of inflammatory signaling in human pre-leukemic disease.

## EXPERIMENTAL PROCEDURES

### Mice and In Vivo Procedures

OCS, *Trp53*$^{f/f}$, and S100A9Tg mice have been previously described (Cheng et al., 2008; Jonkers et al., 2001; Raaijmakers et al., 2010). *Ptprc*$^a$*Pepc*$^b$*/BoyCrl* (B6.SJL) mice were purchased from Charles River. Animals were maintained in specific pathogen free conditions in the Experimental Animal Center of Erasmus MC (EDC). For in vivo cell-cycle analysis, OCS mice received intraperitoneal injections of BrdU (1.5 mg in PBS, BD Biosciences) and sacrificed after 15 hr. For TLR4 studies, 2-week-old mice were intraperitoneally injected with a double dose (100 μg and 35 μg, 48 hr interval) of TLR4-neutralizing antibody (clone MTS510, eBioscience) or isotype control (clone eBR2a, eBioscience) and sacrificed after 60 hr. For NAC rescue studies, 2-week-old mice received daily intraperitoneal injections of NAC (320 mg/kg in saline, Sigma-Aldrich) until the day of the analysis and at least for 5 days. All mice were sacrificed by cervical dislocation. Animal studies were approved by the Animal Welfare/Ethics Committee of the EDC in accordance with legislation in the Netherlands (approval No. EMC 2067, 2714, 2892, 3062).

### μCT Analysis

Femur bones were isolated, fixated in 3% PFA/PBS for 24 hr, and stored in 70% ethanol. μCT analysis was performed using a SkyScan 1172 system (SkyScan) using previously described settings (Tudpor et al., 2015). Bone microarchitectural parameters relative to the trabecular and the cortical area were determined in the distal metaphysis and the middiaphysis of each femur, respectively, using software packages from Bruker MicroCT (NRecon, CTAn, and DataViewer).

### Human Bone Marrow Samples

Bone marrow aspirates were obtained from SDS and DBA patients during routine follow up. All MDS patients were treated with lenalidomide (10 mg/day, d 1–21 in a 4-week schedule) in the context of an ongoing prospective clinical trial for patients with low or intermediate-1 risk MDS according to IPSS criteria (HOVON89; http://www.hovon.nl; http://www.trialregister.nl as NTR1825; EudraCT No. 2008-002195-10). Bone marrow specimens were collected at study entry and disease diagnosis and staging confirmed by central board reviewing. Leukemic evolution was assessed according to WHO criteria; development of RAEB1 or RAEB-2 (if RAEB1 at entry) was considered progression of disease. Leukemia (AML) was diagnosed according to standard WHO criteria ($\geq$20% myeloblasts in blood/bone marrow). Bone marrow cells from allogeneic transplantation donors were used as normal controls. Patients and healthy donor characteristics are described in Tables S4 and S6. All specimens were collected with informed consent, in accordance with the Declaration of Helsinki.

### Gene Expression Profiling

Osx::GFP cells from bone cell suspensions of OCS mice were sorted in TRIzol Reagent (Life Technologies) and RNA was extracted according to the manufacturer's recommendations. Linear amplification of mRNA was performed using the Ovation Pico WTA System (NuGEN). cDNA was fragmented and labeled with Encore Biotin Module (NuGEN). The biotinylated cDNA was hybridized to the GeneChip Mouse Genome 430 2.0 Array (Affymetrix eBioscience). Signal was normalized and differential gene expression analysis was performed with the limma package (Ritchie et al., 2015). RNA sequencing experiments were performed as previously described (Zambetti et al., 2015). Human transcripts were aligned to the RefSeq transcriptome (hg19) and analyzed with DESeq2 (Love et al., 2014), while mouse transcripts were aligned to the Ensembl transcriptome (mm10) and analyzed with EdgeR (Robinson et al., 2010) in the R environment. Fragments per kilobase of transcript per million mapped reads (FPKM) values were calculated using Cufflinks (Trapnell et al., 2010). Principal component analysis was performed in the R environment on the raw fragment counts extracted from the BAM files by HTSeq-count (Anders et al., 2015). For gene set enrichment analysis (Subramanian et al., 2005) (GSEA, Broad Institute), normalized intensity values (microarray data) and FPKM values (RNA-seq) were compared to the curated gene sets (C2) and the gene ontology gene sets (C5) of the Molecular Signature Database (MsigDB) using the Signal2Noise metric and 1,000 gene set-based permutations. For HSPCs gene ontology-term analysis, genes with significantly differential expression ($p < 0.05$) were interrogated using g:Profiler web-based software (Reimand et al., 2007, 2011).

### Immunofluorescence Microscopy

HSPCs were harvested in PBS + 0.5% FBS, cytospun on a glass slide for 3 min at 500 rpm using a Cytospin 4 centrifuge (Thermo Scientific), and fixed in 3% PFA/PBS for 15 min on ice. After three washing steps in PBS, cells were permeabilized for 2 min in 0.15% Triton X-100/PBS. Aspecific binding sites were blocked by incubation in 1% BSA/PBS for 1 hr at room temperature. Cells were

next stained overnight at 4°C with either anti-phospho-histone H2A.X (Ser139) mouse monoclonal antibody (clone JBW301, Merck Millipore, diluted 1:1,000 in 1% BSA/PBS) or with anti-53BP1 rabbit polyclonal antibody (Novus Biologicals, diluted 1:1,000 in 1% BSA/PBS). Slides were washed twice in PBS for 5 min and incubated for 1 hr at 37°C with either Alexa Fluor 488-conjugated goat anti-mouse antibody (Cat. A10667, Life Technologies) or goat anti-rabbit antibody (Cat. A11008, Life Technologies), both diluted 1:200 in 1% BSA/PBS. After two washes in PBS, slides were mounted in VECTASHIELD Mounting Medium with DAPI (Vector Laboratories). z series images were acquired with a Leica TCS SP5 confocal microscope (63× objective lens) using the LAS software (Leica Microsystems). γH2AX and 53BP1 foci were counted manually from the maximum projection view.

### Survival Analysis

The low-risk MDS patient subgroup with S100 niche signature was defined by the Modified Thompson Tau test for outlier detection. In brief, *S100A8* statistics from the control cases were combined to define the rejection region, demarcating FPKM values to be considered as outliers. MDS cases with *S100A8* FPKM values within the rejection region were thus defined as niche-signature$^+$. To determine the significance difference in time to progression, we used the Wilcoxon signed-rank test accounting for tied observations. Event-free survival was determined by specifying leukemic progression or death as events. Patients experiencing a non-hematological related death (e.g., cardiac failure), were censored on the date of this event. Patients remaining alive were censored on the date of last consultation. Kaplan-Meier curves were used to estimate the survival functions through time. Statistical differences in the survival distributions were assessed with the Mantel-Cox log-rank test. All calculations were performed in the R environment.

### Statistics

Statistical analysis was performed using Prism 5 (GraphPad Software). Unless otherwise specified, unpaired, two-tailed Student's t test (single test) or one-way ANOVA (multiple comparisons) were used to evaluate statistical significance, defined as $p < 0.05$. All results in bar graphs are mean value ± SEM.

## ACCESSION NUMBERS

The accession number for the gene expression array data derived from murine Osterix::GFP cells is ArrayExpress: E-MTAB-5023. The accession number for the RNA-seq data derived from murine CD48$^-$/CD48$^+$ LSK cells is European Nucleotide Archive, which is hosted by the EBI: PRJEB15060. The accession number for the RNA-seq data derived from human LR-MDS, SDS, and DBA specimens is European Genome-phenome Archive, which is hosted by the EBI: EGAS00001001926.

## SUPPLEMENTAL INFORMATION

Supplemental Information includes Supplemental Experimental Procedures, seven figures, and six tables and can be found with this article online at http://dx.doi.org/10.1016/j.stem.2016.08.021.

## AUTHOR CONTRIBUTIONS

Conceptualization: N.A.Z. and M.H.G.P.R.; Methodology: N.A.Z., Z.P., S.C., K.J.G.K., M.A.M., E.M.J.B., B.C.J.v.d.E., J.P.T.M.v.L., R.K., T.V., and M.H.G.P.R.; Investigation: N.A.Z., Z.P., S.C., M.A.M., E.M.J.B., M.N.A., P.M.H.V.S., C.S.v.d.L., B.C.J.v.d.E., and T.V.; Resources: T.M.W., E.M.P.C., C.M., P.G.M., J.P.T.M.v.L., I.P.T., T.W.K., R.K., A.A.v.d.L., and T.V.; Data Curation: M.A.S., R.M.H., T.M.W., E.M.P.C., T.W.K., and A.A.v.d.L.; Writing: N.A.Z. and M.H.G.P.R.; Visualization: N.A.Z., Z.P., S.C., and R.M.H.; and Supervision and Funding Acquisition: M.H.G.P.R.

## ACKNOWLEDGMENTS

Professor Johanna M. Rommens donated *Sbds*-floxed mice; Dr. Eric Braakman and Mariette ter Borg provided CD34$^+$ cells; Dr. Elwin Rombouts, Onno Roovers, Peter van Geel, Kirsten van Lom, Marijke Koedam, Nicole van Vliet, Charlie Laffeber, and Gert-Jan Kremers provided technical assistance; Dr. Marc Bierings and Dr. Valerie de Haas on behalf of the "Stichting Kinderoncologie Nederland (SKION)" provided DBA samples; Pearl F.M. Mau Asam helped with SDS bone marrow collection; members of the myeloid working party of HOVON collected MDS bone marrow samples; Dr. Dana Chitu of the HOVON data center helped with clinical data; members of the Erasmus MC Department of Hematology provided scientific discussion; and members of the Erasmus MC animal core facility EDC helped with animal care. This work was supported by grants from the Dutch Cancer Society (KWF Kankerbestrijding), Amsterdam, the Netherlands (grant EMCR 2010-4733 to M.H.G.P.R.), the ErasmusMC (Fellowship to M.H.G.P.R.), the Netherlands Organization of Scientific Research (NWO 90700422 to M.H.G.P.R.), and the Netherlands Genomics Initiative (Zenith grant no 40-41009-98-11062 to M.H.G.P.R.).

Received: November 23, 2015
Revised: July 6, 2016
Accepted: August 22, 2016
Published: September 22, 2016

## REFERENCES

Aggett, P.J., Cavanagh, N.P.C., Matthew, D.J., Pincott, J.R., Sutcliffe, J., and Harries, J.T. (1980). Shwachman's syndrome. A review of 21 cases. Arch. Dis. Child. *55*, 331–347.

Alter, B.P. (2007). Diagnosis, genetics, and management of inherited bone marrow failure syndromes. Hematology (Am. Soc. Hematol. Educ. Program) *1*, 29–39.

Ambekar, C., Das, B., Yeger, H., and Dror, Y. (2010). SBDS-deficiency results in deregulation of reactive oxygen species leading to increased cell death and decreased cell growth. Pediatr. Blood Cancer *55*, 1138–1144.

Anders, S., Pyl, P.T., and Huber, W. (2015). HTSeq–a Python framework to work with high-throughput sequencing data. Bioinformatics *31*, 166–169.

Arranz, L., Sánchez-Aguilera, A., Martín-Pérez, D., Isern, J., Langa, X., Tzankov, A., Lundberg, P., Muntión, S., Tzeng, Y.S., Lai, D.M., et al. (2014). Neuropathy of haematopoietic stem cell niche is essential for myeloproliferative neoplasms. Nature *512*, 78–81.

Austin, K.M., Gupta, M.L., Jr., Coats, S.A., Tulpule, A., Mostoslavsky, G., Balazs, A.B., Mulligan, R.C., Daley, G., Pellman, D., and Shimamura, A. (2008). Mitotic spindle destabilization and genomic instability in Shwachman-Diamond syndrome. J. Clin. Invest. *118*, 1511–1518.

Ball, H.L., Zhang, B., Riches, J.J., Gandhi, R., Li, J., Rommens, J.M., and Myers, J.S. (2009). Shwachman-Bodian Diamond syndrome is a multi-functional protein implicated in cellular stress responses. Hum. Mol. Genet. *18*, 3684–3695.

Bejar, R., Stevenson, K.E., Caughey, B.A., Abdel-Wahab, O., Steensma, D.P., Galili, N., Raza, A., Kantarjian, H., Levine, R.L., Neuberg, D., et al. (2012). Validation of a prognostic model and the impact of mutations in patients with lower-risk myelodysplastic syndromes. J. Clin. Oncol. *30*, 3376–3382.

Boocock, G.R., Morrison, J.A., Popovic, M., Richards, N., Ellis, L., Durie, P.R., and Rommens, J.M. (2003). Mutations in SBDS are associated with Shwachman-Diamond syndrome. Nat. Genet. *33*, 97–101.

Chen, X., Eksioglu, E.A., Zhou, J., Zhang, L., Djeu, J., Fortenbery, N., Epling-Burnette, P., Van Bijnen, S., Dolstra, H., Cannon, J., et al. (2013). Induction of myelodysplasia by myeloid-derived suppressor cells. J. Clin. Invest. *123*, 4595–4611.

Chen, S., Zambetti, N.A., Bindels, E.M., Kenswill, K., Mylona, A.M., Adisty, N.M., Hoogenboezem, R.M., Sanders, M.A., Cremers, E.M., Westers, T.M., et al. (2016). Massive parallel RNA sequencing of highly purified mesenchymal elements in low-risk MDS reveals tissue-context-dependent activation of inflammatory programs. Leukemia, Published online June 3, 2016. http://dx.doi.org/10.1038/leu.2016.91.

Cheng, P., Corzo, C.A., Luetteke, N., Yu, B., Nagaraj, S., Bui, M.M., Ortiz, M., Nacken, W., Sorg, C., Vogl, T., et al. (2008). Inhibition of dendritic cell differentiation and accumulation of myeloid-derived suppressor cells in cancer is regulated by S100A9 protein. J. Exp. Med. *205*, 2235–2249.

Curtin, N.J. (2012). DNA repair dysregulation from cancer driver to therapeutic target. Nat. Rev. Cancer *12*, 801–817.

Donadieu, J., Fenneteau, O., Beaupain, B., Beaufils, S., Bellanger, F., Mahlaoui, N., Lambilliotte, A., Aladjidi, N., Bertrand, Y., Mialou, V., et al.; Associated investigators of the French Severe Chronic Neutropenia Registry* (2012). Classification of and risk factors for hematologic complications in a French national cohort of 102 patients with Shwachman-Diamond syndrome. Haematologica *97*, 1312–1319.

Finch, A.J., Hilcenko, C., Basse, N., Drynan, L.F., Goyenechea, B., Menne, T.F., González Fernández, A., Simpson, P., D'Santos, C.S., Arends, M.J., et al. (2011). Uncoupling of GTP hydrolysis from eIF6 release on the ribosome causes Shwachman-Diamond syndrome. Genes Dev. *25*, 917–929.

Flores-Figueroa, E., Varma, S., Montgomery, K., Greenberg, P.L., and Gratzinger, D. (2012). Distinctive contact between CD34+ hematopoietic progenitors and CXCL12+ CD271+ mesenchymal stromal cells in benign and myelodysplastic bone marrow. Lab. Invest. *92*, 1330–1341.

Gañán-Gómez, I., Wei, Y., Starczynowski, D.T., Colla, S., Yang, H., Cabrero-Calvo, M., Bohannan, Z.S., Verma, A., Steidl, U., and Garcia-Manero, G. (2015). Deregulation of innate immune and inflammatory signaling in myelodysplastic syndromes. Leukemia *29*, 1458–1469.

Ginzberg, H., Shin, J., Ellis, L., Morrison, J., Ip, W., Dror, Y., Freedman, M., Heitlinger, L.A., Belt, M.A., Corey, M., et al. (1999). Shwachman syndrome: phenotypic manifestations of sibling sets and isolated cases in a large patient cohort are similar. J. Pediatr. *135*, 81–88.

Hanoun, M., Zhang, D., Mizoguchi, T., Pinho, S., Pierce, H., Kunisaki, Y., Lacombe, J., Armstrong, S.A., Dührsen, U., and Frenette, P.S. (2014). Acute myelogenous leukemia-induced sympathetic neuropathy promotes malignancy in an altered hematopoietic stem cell niche. Cell Stem Cell *15*, 365–375.

Head, D.R., Jacobberger, J.W., Mosse, C., Jagasia, M., Dupont, W., Goodman, S., Flye, L., Shinar, A., McClintock-Treep, S., Stelzer, G., et al. (2011). Innovative analyses support a role for DNA damage and an aberrant cell cycle in myelodysplastic syndrome pathogenesis. Bone Marrow Res. *2011*, 950934.

Ito, K., Hirao, A., Arai, F., Takubo, K., Matsuoka, S., Miyamoto, K., Ohmura, M., Naka, K., Hosokawa, K., Ikeda, Y., and Suda, T. (2006). Reactive oxygen species act through p38 MAPK to limit the lifespan of hematopoietic stem cells. Nat. Med. *12*, 446–451.

Jaiswal, S., Fontanillas, P., Flannick, J., Manning, A., Grauman, P.V., Mar, B.G., Lindsley, R.C., Mermel, C.H., Burtt, N., Chavez, A., et al. (2014). Age-related clonal hematopoiesis associated with adverse outcomes. N. Engl. J. Med. *371*, 2488–2498.

Jonkers, J., Meuwissen, R., van der Gulden, H., Peterse, H., van der Valk, M., and Berns, A. (2001). Synergistic tumor suppressor activity of BRCA2 and p53 in a conditional mouse model for breast cancer. Nat. Genet. *29*, 418–425.

Kode, A., Manavalan, J.S., Mosialou, I., Bhagat, G., Rathinam, C.V., Luo, N., Khiabanian, H., Lee, A., Murty, V.V., Friedman, R., et al. (2014). Leukaemogenesis induced by an activating β-catenin mutation in osteoblasts. Nature *506*, 240–244.

Li, C., Chen, H., Ding, F., Zhang, Y., Luo, A., Wang, M., and Liu, Z. (2009). A novel p53 target gene, S100A9, induces p53-dependent cellular apoptosis and mediates the p53 apoptosis pathway. Biochem. J. *422*, 363–372.

Li, L., Li, M., Sun, C., Francisco, L., Chakraborty, S., Sabado, M., McDonald, T., Gyorffy, J., Chang, K., Wang, S., et al. (2011). Altered hematopoietic cell gene expression precedes development of therapy-related myelodysplasia/acute myeloid leukemia and identifies patients at risk. Cancer Cell *20*, 591–605.

Love, M.I., Huber, W., and Anders, S. (2014). Moderated estimation of fold change and dispersion for RNA-seq data with DESeq2. Genome Biol. *15*, 550.

Mäkitie, O., Ellis, L., Durie, P.R., Morrison, J.A., Sochett, E.B., Rommens, J.M., and Cole, W.G. (2004). Skeletal phenotype in patients with Shwachman-Diamond syndrome and mutations in SBDS. Clin. Genet. *65*, 101–112.

Maratheftis, C.I., Andreakos, E., Moutsopoulos, H.M., and Voulgarelis, M. (2007). Toll-like receptor-4 is up-regulated in hematopoietic progenitor cells and contributes to increased apoptosis in myelodysplastic syndromes. Clin. Cancer Res. *13*, 1154–1160.

Marino, S., Vooijs, M., van Der Gulden, H., Jonkers, J., and Berns, A. (2000). Induction of medulloblastomas in p53-null mutant mice by somatic inactivation of Rb in the external granular layer cells of the cerebellum. Genes Dev. *14*, 994–1004.

Medyouf, H., Mossner, M., Jann, J.C., Nolte, F., Raffel, S., Herrmann, C., Lier, A., Eisen, C., Nowak, V., Zens, B., et al. (2014). Myelodysplastic cells in patients reprogram mesenchymal stromal cells to establish a transplantable stem cell niche disease unit. Cell Stem Cell *14*, 824–837.

Murphy, M.P. (2009). How mitochondria produce reactive oxygen species. Biochem. J. *417*, 1–13.

Owusu-Ansah, E., Yavari, A., Mandal, S., and Banerjee, U. (2008). Distinct mitochondrial retrograde signals control the G1-S cell cycle checkpoint. Nat. Genet. *40*, 356–361.

Peddie, C.M., Wolf, C.R., McLellan, L.I., Collins, A.R., and Bowen, D.T. (1997). Oxidative DNA damage in CD34+ myelodysplastic cells is associated with intracellular redox changes and elevated plasma tumour necrosis factor-alpha concentration. Br. J. Haematol. *99*, 625–631.

Raaijmakers, M.H., Mukherjee, S., Guo, S., Zhang, S., Kobayashi, T., Schoonmaker, J.A., Ebert, B.L., Al-Shahrour, F., Hasserjian, R.P., Scadden, E.O., et al. (2010). Bone progenitor dysfunction induces myelodysplasia and secondary leukaemia. Nature *464*, 852–857.

Raiser, D.M., Narla, A., and Ebert, B.L. (2014). The emerging importance of ribosomal dysfunction in the pathogenesis of hematologic disorders. Leuk. Lymphoma *55*, 491–500.

Rawls, A.S., Gregory, A.D., Woloszynek, J.R., Liu, F., and Link, D.C. (2007). Lentiviral-mediated RNAi inhibition of Sbds in murine hematopoietic progenitors impairs their hematopoietic potential. Blood *110*, 2414–2422.

Reimand, J., Kull, M., Peterson, H., Hansen, J., and Vilo, J. (2007). g:Profiler–a web-based toolset for functional profiling of gene lists from large-scale experiments. Nucleic Acids Res. *35*, W193–W200.

Reimand, J., Arak, T., and Vilo, J. (2011). g:Profiler–a web server for functional interpretation of gene lists (2011 update). Nucleic Acids Res. *39*, W307–W315.

Ritchie, M.E., Phipson, B., Wu, D., Hu, Y., Law, C.W., Shi, W., and Smyth, G.K. (2015). limma powers differential expression analyses for RNA-sequencing and microarray studies. Nucleic Acids Res. *43*, e47.

Robinson, M.D., McCarthy, D.J., and Smyth, G.K. (2010). edgeR: a Bioconductor package for differential expression analysis of digital gene expression data. Bioinformatics *26*, 139–140.

Rossi, D.J., Bryder, D., Seita, J., Nussenzweig, A., Hoeijmakers, J., and Weissman, I.L. (2007). Deficiencies in DNA damage repair limit the function of haematopoietic stem cells with age. Nature *447*, 725–729.

Sahin, E., and Depinho, R.A. (2010). Linking functional decline of telomeres, mitochondria and stem cells during ageing. Nature *464*, 520–528.

Schepers, K., Pietras, E.M., Reynaud, D., Flach, J., Binnewies, M., Garg, T., Wagers, A.J., Hsiao, E.C., and Passegué, E. (2013). Myeloproliferative neoplasia remodels the endosteal bone marrow niche into a self-reinforcing leukemic niche. Cell Stem Cell *13*, 285–299.

Schepers, K., Campbell, T.B., and Passegué, E. (2015). Normal and leukemic stem cell niches: insights and therapeutic opportunities. Cell Stem Cell *16*, 254–267.

Schneider, R.K., Schenone, M., Ferreira, M.V., Kramann, R., Joyce, C.E., Hartigan, C., Beier, F., Brümmendorf, T.H., Germing, U., Platzbecker, U., et al. (2016). Rps14 haploinsufficiency causes a block in erythroid differentiation mediated by S100A8 and S100A9. Nat. Med. *22*, 288–297.

Srikrishna, G., and Freeze, H.H. (2009). Endogenous damage-associated molecular pattern molecules at the crossroads of inflammation and cancer. Neoplasia *11*, 615–628.

Starczynowski, D.T., Kuchenbauer, F., Argiropoulos, B., Sung, S., Morin, R., Muranyi, A., Hirst, M., Hogge, D., Marra, M., Wells, R.A., et al. (2010). Identification of miR-145 and miR-146a as mediators of the 5q- syndrome phenotype. Nat. Med. *16*, 49–58.

Stowe, D.F., and Camara, A.K.S. (2009). Mitochondrial reactive oxygen species production in excitable cells: modulators of mitochondrial and cell function. Antioxid. Redox Signal. *11*, 1373–1414.

Subramanian, A., Tamayo, P., Mootha, V.K., Mukherjee, S., Ebert, B.L., Gillette, M.A., Paulovich, A., Pomeroy, S.L., Golub, T.R., Lander, E.S., and Mesirov, J.P. (2005). Gene set enrichment analysis: a knowledge-based approach for interpreting genome-wide expression profiles. Proc. Natl. Acad. Sci. USA *102*, 15545–15550.

Toiviainen-Salo, S., Mäyränpää, M.K., Durie, P.R., Richards, N., Grynpas, M., Ellis, L., Ikegawa, S., Cole, W.G., Rommens, J., Marttinen, E., et al. (2007). Shwachman-Diamond syndrome is associated with low-turnover osteoporosis. Bone *41*, 965–972.

Tormin, A., Li, O., Brune, J.C., Walsh, S., Schütz, B., Ehinger, M., Ditzel, N., Kassem, M., and Scheding, S. (2011). CD146 expression on primary nonhematopoietic bone marrow stem cells is correlated with in situ localization. Blood *117*, 5067–5077.

Trapnell, C., Williams, B.A., Pertea, G., Mortazavi, A., Kwan, G., van Baren, M.J., Salzberg, S.L., Wold, B.J., and Pachter, L. (2010). Transcript assembly and quantification by RNA-Seq reveals unannotated transcripts and isoform switching during cell differentiation. Nat. Biotechnol. *28*, 511–515.

Tudpor, K., van der Eerden, B.C., Jongwattanapisan, P., Roelofs, J.J., van Leeuwen, J.P., Bindels, R.J., and Hoenderop, J.G. (2015). Thrombin receptor deficiency leads to a high bone mass phenotype by decreasing the RANKL/OPG ratio. Bone *72*, 14–22.

Vlachos, A., Rosenberg, P.S., Atsidaftos, E., Alter, B.P., and Lipton, J.M. (2012). Incidence of neoplasia in Diamond Blackfan anemia: a report from the Diamond Blackfan Anemia Registry. Blood *119*, 3815–3819.

Vogl, T., Tenbrock, K., Ludwig, S., Leukert, N., Ehrhardt, C., van Zoelen, M.A., Nacken, W., Foell, D., van der Poll, T., Sorg, C., and Roth, J. (2007). Mrp8 and Mrp14 are endogenous activators of Toll-like receptor 4, promoting lethal, endotoxin-induced shock. Nat. Med. *13*, 1042–1049.

Vogl, T., Eisenblätter, M., Völler, T., Zenker, S., Hermann, S., van Lent, P., Faust, A., Geyer, C., Petersen, B., Roebrock, K., et al. (2014). Alarmin S100A8/S100A9 as a biomarker for molecular imaging of local inflammatory activity. Nat. Commun. *5*, 4593.

Walkley, C.R., Olsen, G.H., Dworkin, S., Fabb, S.A., Swann, J., McArthur, G.A., Westmoreland, S.V., Chambon, P., Scadden, D.T., and Purton, L.E. (2007). A microenvironment-induced myeloproliferative syndrome caused by retinoic acid receptor gamma deficiency. Cell *129*, 1097–1110.

Walter, D., Lier, A., Geiselhart, A., Thalheimer, F.B., Huntscha, S., Sobotta, M.C., Moehrle, B., Brocks, D., Bayindir, I., Kaschutnig, P., et al. (2015). Exit from dormancy provokes DNA-damage-induced attrition in haematopoietic stem cells. Nature *520*, 549–552.

Wang, X., Kua, H.Y., Hu, Y., Guo, K., Zeng, Q., Wu, Q., Ng, H.H., Karsenty, G., de Crombrugghe, B., Yeh, J., and Li, B. (2006). p53 functions as a negative regulator of osteoblastogenesis, osteoblast-dependent osteoclastogenesis, and bone remodeling. J. Cell Biol. *172*, 115–125.

Wei, Y., Dimicoli, S., Bueso-Ramos, C., Chen, R., Yang, H., Neuberg, D., Pierce, S., Jia, Y., Zheng, H., Wang, H., et al. (2013). Toll-like receptor alterations in myelodysplastic syndrome. Leukemia *27*, 1832–1840.

Woloszynek, J.R., Rothbaum, R.J., Rawls, A.S., Minx, P.J., Wilson, R.K., Mason, P.J., Bessler, M., and Link, D.C. (2004). Mutations of the SBDS gene are present in most patients with Shwachman-Diamond syndrome. Blood *104*, 3588–3590.

Xiao, Y., Wang, J., Song, H., Zou, P., Zhou, D., and Liu, L. (2013). CD34+ cells from patients with myelodysplastic syndrome present different p21 dependent premature senescence. Leuk. Res. *37*, 333–340.

Yahata, T., Takanashi, T., Muguruma, Y., Ibrahim, A.A., Matsuzawa, H., Uno, T., Sheng, Y., Onizuka, M., Ito, M., Kato, S., and Ando, K. (2011). Accumulation of oxidative DNA damage restricts the self-renewal capacity of human hematopoietic stem cells. Blood *118*, 2941–2950.

Zambetti, N.A., Bindels, E.M., Van Strien, P.M., Valkhof, M.G., Adisty, M.N., Hoogenboezem, R.M., Sanders, M.A., Rommens, J.M., Touw, I.P., and Raaijmakers, M.H. (2015). Deficiency of the ribosome biogenesis gene Sbds in hematopoietic stem and progenitor cells causes neutropenia in mice by attenuating lineage progression in myelocytes. Haematologica *100*, 1285–1293.